MIXER-BASED SUBARRAY BEAMFORMING FOR SUB-NYQUIST SAMPLING ULTRASOUND ARCHITECTURES

Jonathon Spaulding*, Yonina C. Eldar†, Boris Murmann*

* Stanford University, Dept. of Electrical Engineering, Stanford, CA
† Technion - Israel Institute of Technology, Dept. of Electrical Engineering, Haifa, Israel

ABSTRACT

Ultrasound imagers suffer from a large data rate between their analog to digital converter (ADC) front-end and digital beamforming backend. This becomes a limiting factor when the number of elements is increased, such as in modern 2D transducers. To address this issue, prior work considered sub-Nyquist sampling techniques that exploit the disparity between the signal's physical bandwidth and innovation rate. In this work, we extend this framework using an analog-domain subarray beamforming technique that is feasible due to the narrowband nature of the sub-Nyquist signal acquisition. When applied to waveforms taken from a commercial ultrasound machine, this method reduces both the low-rate ADC count by a factor of eight and the total data rate by a factor of 54 with minimal image degradation.

Index Terms— Ultrasound Imaging, Sub-Nyquist Sampling, Subarray Beamforming, Compressed Sensing

1. INTRODUCTION

Modern ultrasound machines use an array of transducer elements to transmit acoustic energy into a target to image its internal structure [1]. Each transducer element receives back a delayed version of the signal, where the delay differences between the elements are determined by geometric time-of-flight (ToF) differences. Using digital beamforming, the received signals are shifted in time to achieve coherent summation, thus increasing the signal-to-noise ratio (SNR). The relatively fine time resolution required comes from a combination of high sampling rates and digital interpolation. In many applications, especially ones involving 2D transducers, the resulting high data rate becomes difficult to manage efficiently.

In light of this issue, several data reduction techniques have been proposed. Bilge et al. trade off frame rate for hardware channel count by only activating small subarrays of receive elements for each firing event [2]. Blaak et al. [3] and Yu et al. [4] divide the array into subarrays, apply fixed delays to each subarray element and sum the delayed signals before digitization. This technique has the benefit of a low-complexity hardware implementation, but subarrays physically distant from the reference do not focus properly. Halvorsrod et al. [5] use a programmable number of analog all-pass filters to delay signals so that they may be summed prior to digitization, which trades hardware complexity against subarray resolution.

In a separate line of work, the problem is approached using analog pre-filtering and sub-Nyquist sampling. The technique proposed by Tur et al. [6] enables substantial reduction in ADC sampling rate,

but requires reconstruction for each transducer signal before conventional beamforming. Wagner et al. [7] solve this issue by applying the beamforming operator in the frequency domain on low-rate signals. Both Wagner et al. [7], followed by Chernyakova et al. [8], demonstrate that frequency-beamformed low-rate signals can be reconstructed using compressed sensing (CS) techniques [9].

The approach described in this paper leverages a combination of subarray beamforming and sub-Nyquist sampling. Our architecture is similar to that of [8], where each received signal is mixed to baseband and passed through a low-pass filter with a cutoff frequency far below the physical signal bandwidth. The narrowband nature of this approach allows us to implement time delays using phase shifts in our mixing signals (see Fig. 1), leading to low-complexity subarray beamforming prior to sub-Nyquist digitization. By allowing these mixing signals to vary between receive channels, we achieve dynamic array focusing on a per element basis. The net result is an architecture with significant reductions in ADC count and data rate, with only minor degradations in image quality.

The remainder of this paper is as follows. Section 2 describes the subarray beamforming technique applied to a dynamically focused imaging system. In Section 3, we explore approximations that enable an efficient hardware implementation. Finally, we evaluate the performance of this method using a combination of real image data and numerical simulations in Section 4 and draw conclusions in Section 5.
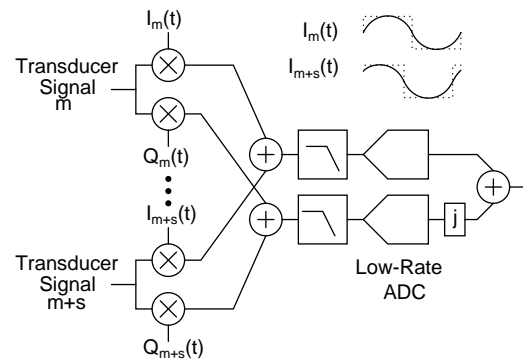
Fig. 1: Mixer-based subarray beamforming architecture with two ADCs per subarray, consisting of array elements m through $m + s$.

2. DYNAMIC SUBARRAY BEAMFORMING

Consider a pulse that is transmitted at time $t = 0$, orthogonal to the array with beamforming reference coordinate δ_f in a conventional linear array (see Fig. 2). For a reflection occurring at time $t \geq 0$,

each element m in the array receives the reflection at time

$$\tau_m(t) = t + \sqrt{t^2 + \gamma_m^2} \qquad (1)$$

where $\gamma_m = \frac{\delta_m - \delta_f}{c}$, δ_m is the array coordinate of element m, and c is the acoustic velocity of the target (assumed constant). The signal at the beamforming reference sees $\tau_f = 2t$. For each element in an array, linear beamforming delays the received signal of the mth element ($\phi_m(t)$) so that the resulting signal $\hat{\phi}_m(t)$ is aligned with that of the reference

$$\hat{\phi}_m(t) = \phi_m\left(\tau_m\left(\frac{t}{2}\right)\right). \qquad (2)$$

The resulting delayed signals are now added, resulting in the beamformed signal for the scanline. It was shown in [7] that this operation can be performed in the frequency domain by computing the Fourier coefficients of the aligned signal $\hat{\Phi}_m[k]$ as a convolution product between the Fourier coefficients of the unaligned signal $\Phi_m[k]$ and an *a priori* known beamforming kernel $Q_{m,k}[n]$ which is derived from $\tau_m(t)$:

$$\hat{\Phi}_m[k] = \sum_n \Phi_m[k-n]Q_{m,k}[n]. \qquad (3)$$

Our subarray beamforming method splits this operation into two stages. The subarray beamforming operation aligns and adds the received signals from each subarray element in the analog domain. We then combine the resulting subarray signals after sub-Nyquist sampling using the frequency-domain techniques from [7] and [8].

The alignment equations for subarray beamforming differ from (1) as we align the received signals from each element within a subarray to the center of that subarray, δ_s, instead of to the global reference δ_f. This results in the requirement that the subarray aligned signal $\hat{\phi}_m(t)$ satisfies

$$\hat{\phi}_m(t + \sqrt{t^2 + \gamma_s^2}) = \phi_m(t + \sqrt{t^2 + \gamma_m^2}) \qquad (4)$$

where $\gamma_s = \frac{\delta_s - \delta_f}{c}$ indicates the ToF between element m's subarray center δ_s and the global beamforming reference δ_f, and $\gamma_m = \frac{\delta_m - \delta_f}{c}$. This is equivalent to the statement

$$\hat{\phi}_m(t) = \phi_m(\tau_m(t))$$
$$\tau_m(t) = \frac{t^2 - \gamma_s^2}{2t} + \sqrt{\left(\frac{t^2 - \gamma_s^2}{2t}\right)^2 + \gamma_m^2}. \qquad (5)$$

The so-aligned signals are added to produce one signal per subarray, which are then further combined using the methods from [8] assuming a new effective array with elements located at the points δ_s. If $\phi_m(t)$ is periodic with period T, the Fourier coefficients of the signal after subarray beamforming, $\hat{\Phi}_m[k]$, can be written as

$$\hat{\Phi}_m[k] = \frac{1}{T}\int_0^T \phi_m(\tau_m(t))e^{-j2\pi kt/T}dt. \qquad (6)$$

Following a similar derivation to the one in [7], the Fourier coefficients of a subarray beamformed signal can be expressed as

$$\hat{\Phi}_m[k] = \frac{1}{T}\int_0^T \phi_m(t)q_{m,k}(t)e^{-j2\pi kt/T}dt \qquad (7)$$
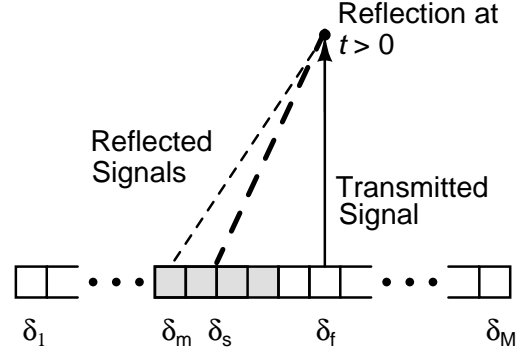
Fig. 2: M-element 1D linear array beamforming geometry with 4-element shaded subarray.

with

$$q_{m,k}(t) = g_{m,k}(t)\frac{1}{2}\left(1 + \frac{\gamma_m^2}{t^2} + \frac{1/2(t - \gamma_m^4/t^3)}{\sqrt{\left(\frac{t^2-\gamma_m^2}{2t}\right)^2 + \gamma_s^2}}\right) \qquad (8)$$

and

$$g_{m,k}(t) = e^{-j2\pi k/T\left(\frac{-t}{2} - \frac{\gamma_m^2}{2t} + \sqrt{\left(\frac{t^2-\gamma_m^2}{2t}\right)^2 + \gamma_s^2}\right)}. \qquad (9)$$

The subarray beamformed Fourier coefficients can be described using the same form as (3), with $Q_{m,k}[n]$ indicating the Fourier coefficients of the subarray beamforming signal $q_{m,k}(t)$ given transducer m and desired coefficient k.

The work of [8] demonstrated that an accurate CS reconstruction of ultrasound signals is possible given a partial set of Fourier coefficients $\mathbb{K}$ within the signal bandwidth of a beamformed signal. To implement the result of (4) in hardware, we approximate the function $q_{m,k}[n]$ to remove the dependence on k by using a single coefficient $k = \bar{\mathbb{K}}$. Additionally, the time-dependent gain term in $q_{m,k}(t)$ is approximated as unity so that

$$q_{m,k}(t) \approx g_{m,\bar{\mathbb{K}}}(t). \qquad (10)$$

The approximation of (10) allows us to implement subarray beamforming by multiplying the signals $g_{m,\bar{\mathbb{K}}}(t)$ with each transducer's received signal. Setting $k = \bar{\mathbb{K}}$ is a narrowband approximation, which is enabled by the fact that we are estimating only a partial set of Fourier coefficients from the signal bandwidth as well as by the fact that the implemented delays are small. The error caused by this approximation increases as more Fourier coefficients are used or the required delay increases. The delays for elements within a subarray are much smaller than the delays across a full array due to spatial proximity. Fig. 3 plots the average error caused by the approximation (10) for a 64-element linear array with a pitch of 0.29 mm, where the error is defined by (11). The approximation error was calculated for subarrays of size four, and the case where (10) is applied to the full array.

$$\text{Error} = 20\log_{10}\left(\frac{1}{|\mathbb{K}|}\sum_{k\in\mathbb{K}}|Q_{m,k}[n] - G_{m,\bar{\mathbb{K}}}[n]|\right). \qquad (11)$$

Here, the term $Q_{m,k}[n]$ denotes the Fourier coefficients of an ideally beamformed signal, and $G_{m,\mathbb{K}}[n]$ represent the Fourier coefficients resulting from the approximation in (10) followed by global beamforming based on the subarray positions δ_s. The error was averaged
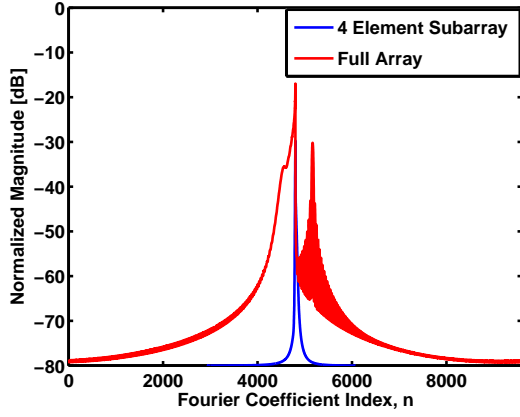
Fig. 3: Error caused by the approximation in (10) for element $m = 1$ in a 64-element array, by coefficient number n, $|\mathbb{K}| = 101$.

for a set of $|\mathbb{K}| = 101$ Fourier coefficients within the signal band, with $T = 210$ μs. We observe from Fig. 3 that the error for a subarray of size four is small compared to the (fictitious) case where (10) is applied to the full array.

3. HARDWARE IMPLEMENTATION

This section considers further approximations to (10) that enable a low-complexity hardware implementation. First, the expression in (7) is multiplied with a complex exponential of frequency f_0. This allows for the selection and baseband processing of Fourier coefficients from anywhere in the spectrum:

$$\tilde{\Phi}_m[k] = \frac{1}{T} \int_0^T \phi_m(t) g_{m,\mathbb{K}}(t) e^{-j2\pi f_0 t} e^{-j2\pi kt/T} dt$$

$$= \sum_n \Phi_m[k + f_0 T - n] G_{m,\bar{\mathbb{K}}}[n]. \quad (12)$$

Multiplying $\phi_m(t)$ by the complex exponentials $g_{m,\mathbb{K}}(t)e^{-j2\pi f_0 t}$ corresponds to a quadrature mixing scheme in hardware:

$$g_{m,\mathbb{K}}(t)e^{-j2\pi f_0 t} = (I_m(t) + jQ_m(t)) \quad (13)$$

with mixing signals as shown in Fig. 1

$$I_m(t) = \cos(2\pi f_0 t + \theta_m(t))$$
$$Q_m(t) = -\sin(2\pi f_0 t + \theta_m(t)) \quad (14)$$

containing a time-varying phase term according to (9)

$$\theta_m(t) = \frac{2\pi\bar{\mathbb{K}}}{T}\left(-\frac{t}{2} - \frac{\gamma_m^2}{2t} + \sqrt{\left(\frac{t^2 - \gamma_m^2}{t}\right)^2 + 4\gamma_s^2}\right). \quad (15)$$

This formulation uses time-varying phase shifts in the mixing signals to implement the desired subarray beamforming delay. As presented, (13)-(15) calls for active (linear) mixers and the generation of sinusoidal signals with time varying phase shifts, both of which are unattractive from a hardware perspective. Therefore, we introduce a final approximation in which the sinusoids are replaced by digitally synthesizable square waves (see Fig. 1). This approach is commonly taken in radio receivers and allows the use of passive switching mixers [10]. The downside of this approach is that it introduces additional mixing terms stemming from the harmonics of
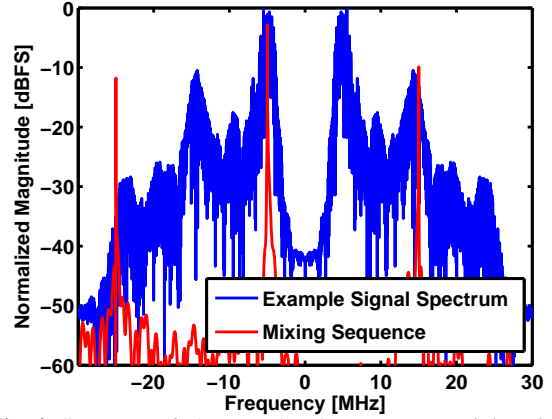

Fig. 4: Spectrum of ultrasound and square wave mixing signals.

the square wave. However, as illustrated in Fig. 4, a typical ultrasound signal contains limited energy at the harmonic mixing frequencies. As demonstrated in the following section, we see only a small amount of out of band signal folding into the set of desired Fourier coefficients, leading to negligible image degradation.

4. SIMULATIONS

To validate the proposed approximations, experiments were run on sampled waveforms from a commercial ultrasound machine. A 96-element linear array probe with 0.295 mm element pitch and center frequency of 2.5 MHz was used. A square wave pulse with period 250 ns was used for transmit. Waveforms from a commercial phantom were sampled by a Verasonics machine (Verasonics, Inc., Redmond, WA) at a rate of 15 MS/s, with an image depth of 10.5 cm, for a total of 2048 samples.
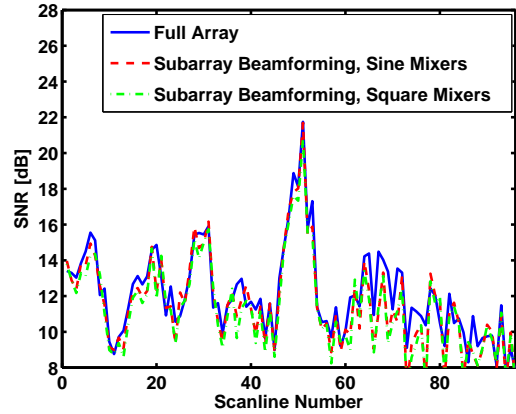
Fig. 5: Accuracy of sub-Nyquist beamforming compared to conventional beamforming. $|\mathbb{K}| = 101$ Fourier coefficients were compared in each scanline and four element subarrays were used.

We first evaluate the accuracy of the low-rate frequency-domain beamforming method from [8], and the subarray beamforming approximations of the previous section relative to conventional time-domain beamforming. Accuracy is measured via SNR (16), where we compare a set of Fourier coefficients from conventionally beamformed signals $\hat{\Phi}$ against the same set of Fourier coefficients resulting from the different beamforming approximations, $\tilde{\Phi}$.

$$\text{SNR} = 20\log_{10} \frac{\|\hat{\mathbf{\Phi}}\|_2}{\|\tilde{\mathbf{\Phi}} - \hat{\mathbf{\Phi}}\|_2} \qquad (16)$$

In each case, a set of $|\mathbb{K}| = 101$ Fourier coefficients is compared. In each of the sub-Nyquist cases, this translates to each ADC taking 141 samples, 101 for the Fourier coefficients, and 40 additional samples for frequency-domain beamforming as discussed in [8]. For the frequency-domain beamforming process from [8], this results in a total sample count reduction of 7.2x when compared to the conventional case. Using four element subarrays, this results in a sample count reduction of 29x. The results as a function of scanline are presented in Fig. 5. By using square wave mixing we observed a penalty of less than 1.5 dB in accuracy when compared to the frequency-domain beamforming technique.

To show that this Fourier coefficient degradation has little impact on image quality, we compare images produced by each of the above beamforming methods against those produced by conventional beamforming. In each sub-Nyquist case, the beamformed scanline was reconstructed using the NESTA algorithm [11]. Fig. 6 compares the conventional beamforming case to the case where subarray beamforming is used with the square wave mixing signals. We make a quantitative measurement of image quality by computing the normalized root-mean-square-error (NRMSE) on a per scanline basis. NRMSE was calculated after performing a Hilbert transform, denoted by $\text{H}(\cdot)$, on the beamformed signal for envelope detection. The NRMSE is calculated by comparing the the conventionally beamformed signal for the jth scanline, $\phi[n,j]$ against each beamformed signal post-reconstruction, $\tilde{\phi}[n,j]$:

$$\text{NRMSE} = \frac{1}{J} \sum_{j=1}^{J} \frac{\sqrt{\frac{1}{N}\sum_{n=1}^{N}(\text{H}(\phi[n,j]) - \text{H}(\tilde{\phi}[n,j]))^2}}{\text{H}(\phi[n,j])_{max} - \text{H}(\phi[n,j])_{min}} \quad (17)$$

where $\text{H}(\Phi[n,j])_{max}$ and $\text{H}(\Phi[n,j])_{min}$ represent the maximum and minimum values for the envelope of the beamformed signal.

After log-compression to 30 dB for display purposes, the images are also compared using the structural similarity (SSIM) index [12]. As shown in Table 1, little difference in image quality is seen between the different beamforming methods when a subarray size of four is used. These results indicate that we can reduce the total number of samples taken (when compared to frequency-domain beamforming) without incurring additional image degradation.

Table 1: NRMSE and SSIM comparisons to the conventionally beamformed ultrasound image of Fig. 6(a)

Method	NRMSE	SSIM
Full Frequency-Domain Beamforming	0.0768	0.6925
Subarray Beamforming, Sine Mixing	0.0763	0.6928
Subarray Beamforming, Square Mixing	0.0762	0.6887

As a final experiment, we test the degradation of image SSIM as a function of subarray size with square wave mixing. Two reconstructions were run, one using $|\mathbb{K}| = 201$ with 100 additional samples taken for the frequency-domain beamforming operation, and one using $|\mathbb{K}| = 101$ with 40 beamforming samples. Fig. 7 calculates the SSIM between reconstructed and conventional images for different subarray sizes. The reconstruction with $|\mathbb{K}| = 201$ demonstrates higher overall performance, and increased sensitivity to subarray size when compared to the reconstruction with $|\mathbb{K}| = 101$. This is to be expected, as this example has fewer errors introduced
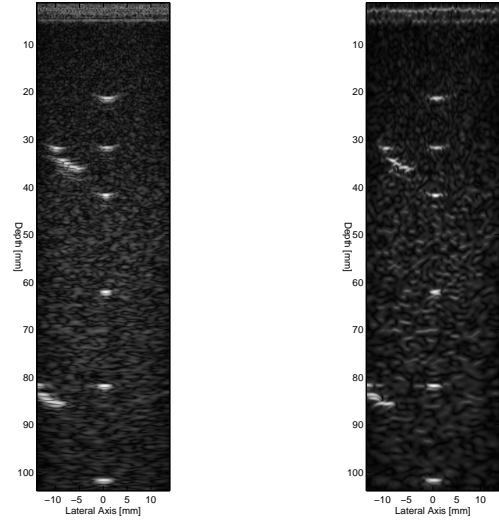
(a) Conventional beamforming   (b) CS subarray beamforming
Fig. 6: Phantom image using (a) conventionally beamforming and (b) and subarray beamforming with square wave mixing and CS reconstruction (29x sample reduction).

from the frequency-domain beamforming operation and the CS reconstruction. For subarray size of 16, we achieve a 54x and 116x reduction of data, respectively, when compared to the conventional case.
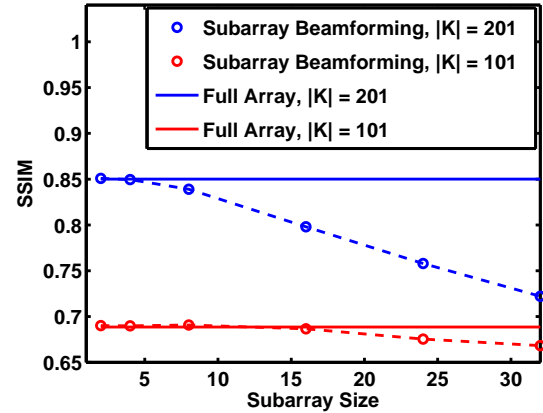
Fig. 7: Image SSIM as a function of subarray size.

5. CONCLUSIONS

To take advantage of increasing transducer element counts, emerging ultrasound imaging applications require solutions that reduce data rates. This work leverages the narrowband nature of a previously proposed sub-Nyquist sampling technique to enable further data rate reductions and hardware simplifications using mixer-based subarray beamforming. Approximating the mixing signals with square waves enables the use of passive switching mixers while introducing negligible image degradation. The proposed method enables a reduction in both ADC count and total data rate by a factor of 16 over previous CS techniques while maintaining similar reconstruction accuracy.

6. REFERENCES

[1] S.W. Smith, Jr. Pavy, H.G., and O.T. Von Ramm, "High-speed ultrasound volumetric imaging system. i. transducer design and beam steering," *Ultrasonics, Ferroelectrics, and Frequency Control, IEEE Transactions on*, vol. 38, no. 2, pp. 100–108, March 1991.

[2] H.S. Bilge and M. Karaman, "Subarray delta-sigma beamforming for ultrasonic imaging," in *Ultrasonics Symposium, 2002. Proceedings. 2002 IEEE*, Oct 2002, vol. 2, pp. 1623–1626 vol.2.

[3] S. Blaak, Z. Yu, G.C.M. Meijer, C. Prins, C.T. Lancee, J.G. Bosch, and N. de Jong, "Design of a micro-beamformer for a 2d piezoelectric ultrasound transducer," in *Ultrasonics Symposium (IUS), 2009 IEEE International*, Sept 2009, pp. 1338–1341.

[4] Z. Yu, S. Blaak, C. Prins, Z. Chang, C.T. Lancee, J.G. Bosch, N. De Jong, G.C.M. Meijer, and M.AP. Pertijs, "A 9-channel low-power receiver asic for 3d transesophageal echocardiography," in *Ultrasonics Symposium (IUS), 2012 IEEE International*, Oct 2012, pp. 2063–2066.

[5] T. Halvorsrod, W. Luzi, and T.S. Lande, "A log-domain beamformer for medical ultrasound imaging systems," *Circuits and Systems I: Regular Papers, IEEE Transactions on*, vol. 52, no. 12, pp. 2563–2575, Dec 2005.

[6] R. Tur, Y.C. Eldar, and Z. Friedman, "Innovation rate sampling of pulse streams with application to ultrasound imaging," *Signal Processing, IEEE Transactions on*, vol. 59, no. 4, pp. 1827–1842, April 2011.

[7] N. Wagner, Y.C. Eldar, and Z. Friedman, "Compressed beamforming in ultrasound imaging," *Signal Processing, IEEE Transactions on*, vol. 60, no. 9, pp. 4643–4657, Sept 2012.

[8] T. Chernyakova and Y. Eldar, "Fourier-domain beamforming: the path to compressed ultrasound imaging," *Ultrasonics, Ferroelectrics, and Frequency Control, IEEE Transactions on*, vol. 61, no. 8, pp. 1252–1267, August 2014.

[9] Y.C. Eldar and G. Kutyniok, *Compressed Sensing: Theory and Applications*, Cambridge University Press, May 2012.

[10] T. Lee, *The Design of CMOS Radio-Frequency Integrated Circuits, Second Edition*, Cambridge University Press, 2003.

[11] Becker, S., Bobin, J., Candes, E., "NESTA: a Fast and Accurate First-Order Method for Sparse Recovery," *SIAM Journal on Imaging Sciences*, 2007.

[12] Wang, Z., Bovik, A., Sheikh, H., Simoncelli, E., "Image Quality Assessment: From Error Visibility to Structural Similarity," *IEEE Transactions on Image Processing*, 2004.